8-1-2005

Microfocal X-Ray Computed Tomography Post-Processing Operations for Optimizing Reconstruction Volumes of Stented Arteries During 3D Computational Fluid Dynamics Modeling

John F. LaDisa
Marquette University, john.ladisa@marquette.edu

Lars E. Olson
Marquette University, lars.olson@marquette.edu

Kristina M. Ropella
Marquette University, kristina.ropella@marquette.edu

Robert C. Molthen
Marquette University, robert.molthen@marquette.edu

Steven Thomas Haworth
Medical College of Wisconsin

Accepted version. *Computer Methods and Programs in Biomedicine*, Vol. 79, No. 2 (August 2005): 121-134. DOI.
John F. LaDisa, Jr. was also affiliated with the Departments of Anesthesiology, Medical College of Wisconsin and the Clement J. Zablocki Veterans Affairs Medical Center at time of publication.
Robert C. Molthen was also affiliated with the Department of Pulmonary and Critical Care Medicine, Medical College of Wisconsin and the Clement J. Zablocki Veterans Affairs Medical Center at time of publication.
David C. Warltier was also affiliated with the Departments of Anesthesiology, Medical College of Wisconsin, Department of Pulmonary and Critical Care Medicine, Medical College of Wisconsin Department of Medicine, Division of Cardiovascular Diseases, Medical College of Wisconsin and the Clement J. Zablocki Veterans Affairs Medical Center at time of publication.

See next page for additional authors

Microfocal X-Ray Computed Tomography Post-Processing Operations for Optimizing Reconstruction Volumes of Stented Arteries During 3D Computational Fluid Dynamics Modeling

John F. LaDisa Jr.
Department of Biomedical Engineering, Marquette University
Departments of Anesthesiology, Medical College of Wisconsin and the Clement J. Zablocki Veterans Affairs Medical Center, Milwaukee, WI
Lars E. Olson
Department of Biomedical Engineering, Marquette University, Milwaukee, WI
Kristina M. Ropella
Department of Biomedical Engineering, Marquette University, Milwaukee, WI

Computer Methods and Programs in Biomedicine, Vol. 79, No. 2 (August 2005): pg. 121-134. DOI.

Robert C. Molthen

Department of Biomedical Engineering, Marquette University Department of Pulmonary and Critical Care Medicine, Medical College of Wisconsin and the Clement J. Zablocki Veterans Affairs Medical Center, Milwaukee, WI

Steven T. Haworth

Department of Pulmonary and Critical Care Medicine, Medical College of Wisconsin and the Clement J. Zablocki Veterans Affairs Medical Center, Milwaukee, WI

Judy R. Kersten

Departments of Anesthesiology, Medical College of Wisconsin and the Clement J. Zablocki Veterans Affairs Medical Center, Department of Pharmacology and Toxicology, Medical College of Wisconsin and the Clement J. Zablocki Veterans Affairs Medical Center, Milwaukee, WI,

David C. Warltier

Department of Biomedical Engineering, Marquette University, Departments of Anesthesiology, Medical College of Wisconsin and the Clement J. Zablocki Veterans Affairs Medical Center, Department of Medicine, Division of Cardiovascular Diseases, Medical College of Wisconsin and the Clement J. Zablocki Veterans Affairs Medical Center, Department of Pharmacology and Toxicology, Medical College of Wisconsin and the Clement J. Zablocki Veterans Affairs Medical Center, Milwaukee, WI

Paul S. Pagel*

Department of Biomedical Engineering, Marquette University, Departments of Anesthesiology, Medical College of Wisconsin and the Clement J. Zablocki Veterans Affairs Medical Center, Milwaukee, WI,

Computer Methods and Programs in Biomedicine, Vol. 79, No. 2 (August 2005): pg. 121-134. DOI.

Summary: Restenosis caused by neointimal hyperplasia (NH) remains an important clinical problem after stent implantation. Restenosis varies with stent geometry, and idealized computational fluid dynamics (CFD) models have indicated that geometric properties of the implanted stent may differentially influence NH. However, 3D studies capturing the in vivo flow domain within stented vessels have not been conducted at a resolution sufficient to detect subtle alterations in vascular geometry caused by the stent and the subsequent temporal development of NH. We present the details and limitations of a series of post-processing operations used in conjunction with microfocal X-ray CT imaging and reconstruction to generate geometrically accurate flow domains within the localized region of a stent several weeks after implantation. Microfocal X-ray CT reconstruction volumes were subjected to an automated program to perform arterial thresholding, spatial orientation, and surface smoothing of stented and unstented rabbit iliac arteries several weeks after antegrade implantation. A transfer function was obtained for the current post-processing methodology containing reconstructed 16 mm stents implanted into rabbit iliac arteries for up to 21 days after implantation and resolved at circumferential and axial resolutions of 32 and 50 μm, respectively. The results indicate that the techniques presented are sufficient to resolve distributions of WSS with 80% accuracy in segments containing 16 surface perturbations over a 16 mm stented region. These methods will be used to test the hypothesis that reductions in normalized wall shear stress (WSS) and increases in the spatial disparity of WSS immediately after stent implantation may spatially correlate with the temporal development of NH within the stented region.

Keywords: Restenosis; Neointimal hyperplasia; Stent

1. Introduction

Experimental and clinical evidence has established a strong correlation between alterations in local vascular geometry, indices of wall shear stress (WSS), and vascular pathology including atherosclerosis and neointimal hyperplasia after stent implantation and angioplasty[1,2]. Computational modeling of regional blood flow through normal or diseased arterial segments requires highly accurate representations of vascular geometry. Our laboratory has conducted several investigations examining theoretical alterations in WSS produced by stent implantation using 3D computational fluid dynamics (CFD) modeling[3,4]. These data suggest that stent design plays an important role in the distribution of low WSS that has been previously correlated with neointimal hyperplasia. However, CFD studies of the flow domain within stented vessels in vivo have yet to be performed with sufficient resolution to identify subtle changes in vascular geometry caused by the progressive development of neointimal

hyperplasia or restenosis after stent implantation[5,6]. Microfocal X-ray computed tomography (CT) imaging provides a rapid means of capturing detailed geometric information within stented vascular segments. We have recently used this technique to examine the correlation between altered indices of WSS and neointimal hyperplasia after stent implantation in rabbit iliac arteries[7] using a previously developed, automated cone-beam reconstruction algorithm[8,9]. The iliac arteries reconstructed using this method contain important geometric information, but modest surface irregularities are introduced during the reconstruction process that compromise more detailed analysis. Thus, we developed a series of post-processing steps to remove these artifacts, but preserve the unique geometric perturbations within the stented region of rabbit iliac arteries several weeks after implantation. In this report, we present the details of these post-processing techniques and describe their validation and potential limitations.

2. Methods

Five general criteria were established as guidelines for acceptable surface smoothing of reconstructed iliac arteries before the development of the post-processing methodology. These guidelines were created to ensure accurate, precise, unbiased, and timely processing of isotropic reconstruction volumes. First, smoothing of the reconstructed iliac arteries was to be performed using previously established and validated techniques. Second, we assumed that computational representations of the iliac artery flow domain should appear smooth in the unstented portion of vessels adjacent to the stented region, but maintain geometric disparity within the stented region of the vessel. Third, we assumed that a phantom vessel (polyethylene 240 tubing) was smooth and had absorption properties similar to a plastic cast of an iliac artery. We further assumed that deviations in normalized distributions of WSS after processing of the reconstructed polyethylene tube should be similar to those described by Moore et al.[10], who also used a phantom vessel to test the influence of various smoothing and computational processing steps on resulting distributions of WSS. Fourth, we imaged all iliac arteries on the same experimental day. If additional time was required to complete microfocal X-ray CT image acquisition, the imaging parameters were consistent across all imaging sessions. Finally, all computational

Computer Methods and Programs in Biomedicine, Vol. 79, No. 2 (August 2005): pg. 121-134. DOI.

representations of the iliac artery flow domain were processed identically using automated image processing programs that were free of user intervention that may inappropriately bias the resulting computational geometries.

2.1. Use and care of animals

All experimental procedures and protocols used in this investigation were approved by the Animal Care and Use Committee of Marquette University and the Medical College of Wisconsin. Furthermore, all conformed to the *Guiding Principles in the Care and Use of Animals* of the American Physiological Society and the *Guide for the Care and Use of Laboratory Animals* as outlined by the National Institutes of Health (7th ed. Washington, DC: Nat. Acad. Press, 1996).

2.2. Iliac artery casting

Antegrade stent implantation was performed as described elsewhere[11]. Rabbits were sacrificed using an intravenous overdose of sodium pentobarbital (10 mg/kg) before microfocal X-ray CT imaging was conducted. The abdomen was opened with a midline incision and a fluid-filled catheter was inserted into the distal aorta. Heparinized saline was then administered to prevent thrombus formation. Peripheral aortic and iliac artery branches were ligated. The internal iliac arteries remained intact because pilot experiments indicated that ligation of these arteries introduced anatomical distortion near the bifurcation. Silk ligatures were placed beneath the proximal portion of each femoral artery for subsequent use during the casting procedure, and the distal portion of each femoral artery was incised to minimize resistance to the flow of casting media. Baton's no. 17 corrosion compound (Polysciences Inc., Warrington, PA, www.polysciences.com) was then injected into the distal aorta and iliac arteries using a perfusion pressure of 100 mm Hg and the femoral arteries were ligated proximally. After curing, the artery and connective tissue were caustically removed (polysciences maceration solution) leaving the flow domain cast and stent. The stent was removed, and small branches were removed[12] using a deformable 300 grit sanding pad leaving the flow domain in the distal aorta and iliac arteries (Fig. 1).

Computer Methods and Programs in Biomedicine, Vol. 79, No. 2 (August 2005): pg. 121-134. DOI.

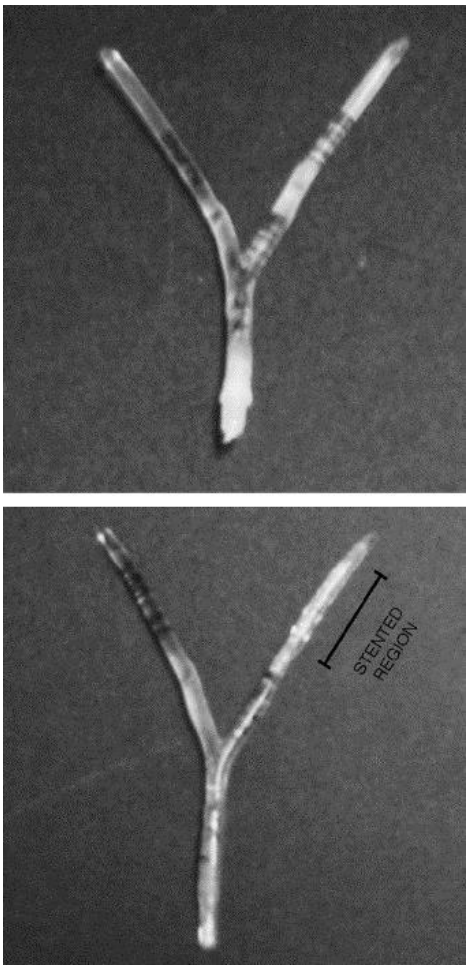

Fig. 1. Representative plastic casts of iliac arteries obtained 21 days after antegrade iliac artery stent implantation in rabbits. The top cast was obtained from a rabbit in which neither iliac artery was stented. The bottom cast was obtained after unilateral implantation of a 16 mm slotted-tube stent in the right iliac artery.

2.3. Microfocal X-ray computed tomography and vascular reconstruction

The iliac artery casts were imaged using a microfocal X-ray CT imaging system. Geometrically accurate reconstruction volumes were generated using the Feldcamp cone-beam reconstruction algorithm[13]. Data acquisition, pre-processing and reconstruction were implemented in a similar fashion to the method described by Karau et al.[8,9] with the addition of a ring artifact reduction (RAR) algorithm[14]. Briefly, the iliac artery casts were inverted and placed on a rotating stage within the X-ray beam (Fig. 2). Thirty projection images were captured and averaged to generate a single image at each of 360 rotation angles

Computer Methods and Programs in Biomedicine, Vol. 79, No. 2 (August 2005): pg. 121-134. DOI.

obtained in one-degree increments (Fig. 3). Spatial errors caused by the magnification process within the image intensifier were removed as previously described[8,9]. The images were then aligned along the center of rotation and processed to remove any spatial and temporal heterogeneity in the X-ray beam.

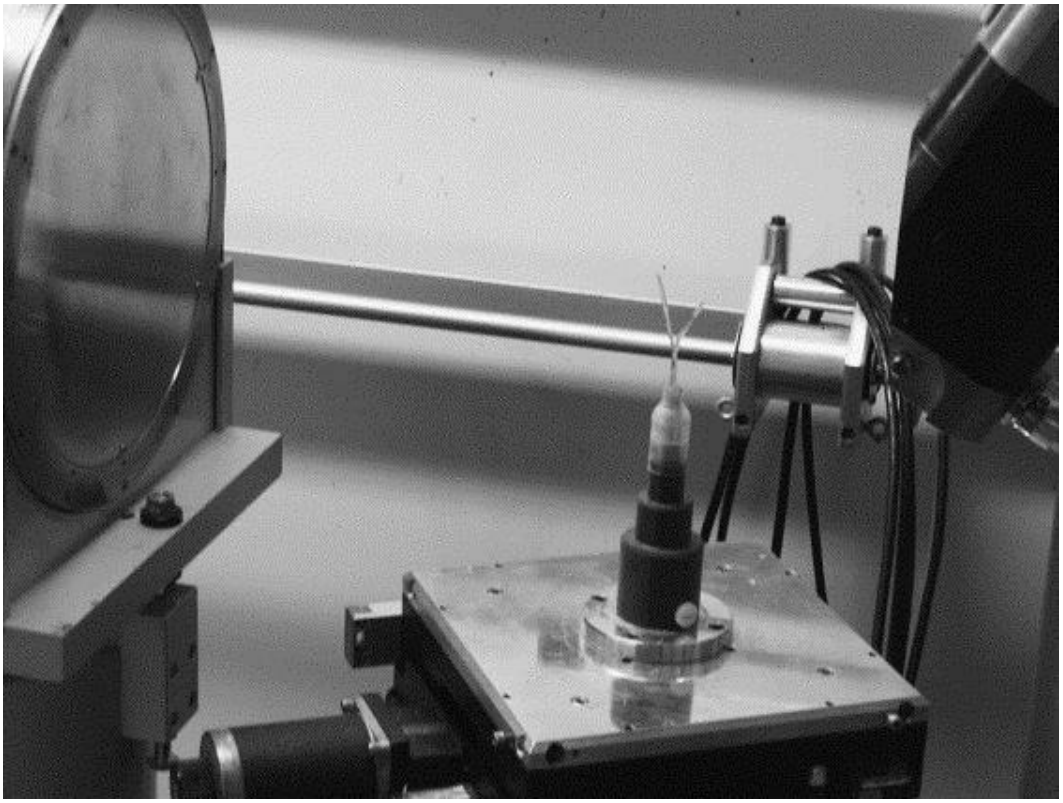

Fig. 2. Microfocal X-ray CT imaging system and cast of a rabbit distal aorta and iliac arteries.

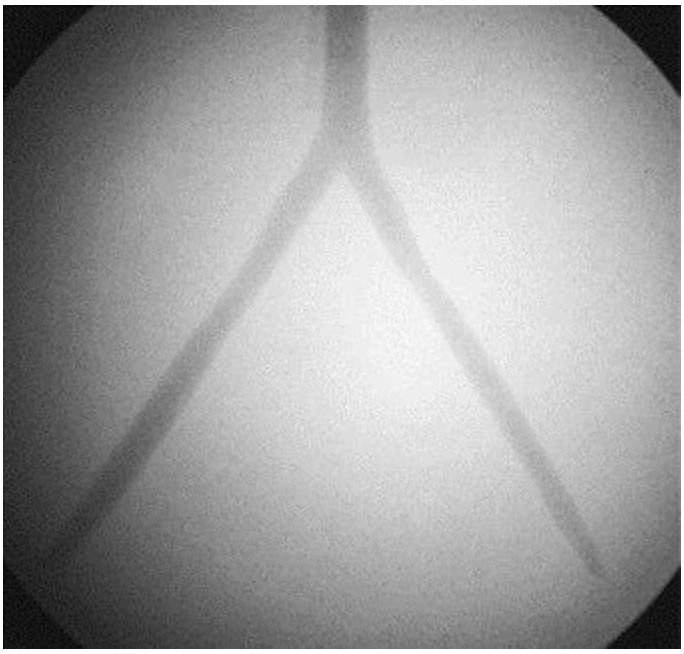

Fig. 3. Representative projection image obtained from an iliac artery cast. Three hundred and sixty such images were obtained for each iliac artery in 1° increments and used to generate isotropic reconstruction volumes.

A charge-coupled device camera captured the images produced by the image intensifier. Camera pixels with non-linear gain or non-zero offset characteristics may introduce circular streaking artifacts that are evident when the reconstruction volume is sectioned perpendicular to the axis of rotation. These artifacts are more prominent under low contrast imaging conditions such as those present in the current report. Anomalous detector pixels may create artifacts near the region of interest and may be misinterpreted as part of the reconstructed iliac artery cast. Such artifacts were eliminated using a previously validated generalized RAR algorithm[14] before cone-beam reconstruction of the casts.

The averaged projection images from each rotation angle were reconstructed to produce isotropic volumes containing 122,763,473 (497^3) voxels[8,9]. High magnification reconstruction volumes were also generated to increase the geometric magnification within the stented portion of the vessel. The subsequent generation of detailed computational meshes used geometric information from a combination of the low and high magnification reconstructions. Polyethylene tubing of a known diameter was inserted at the base of each artery for use in calibration during the reconstruction. The source-to-artery distances

were approximately 15 and 30 cm for the low and high magnification scans, respectively, and the distance from the X-ray source to the image intensifier was approximately 91 cm. Reconstructed vascular volumes were rendered using commercially available software (Analyze 5.0, AnalyzeDirect, Lenexa, KS).

2.4. Reconstructed vascular geometry extraction

Reconstructed volumes were subjected to a series of post-processing operations in preparation for determining distributions of WSS including iliac artery thresholding for identification of the arterial wall, spatial sorting of points along the luminal surface and circumferential and axial surface smoothing. Reconstructed volumes were digitally sectioned perpendicular to the axis of rotation to generate 497 unsigned 8-bit integer arrays using Unix script files. The images were then adjusted to use the full dynamic range (0–255 grayscale levels), and an image threshold was implemented using an automated program designed in Matlab. Discontinuities within the binary images were filled using the *imfill* function within the image processing toolbox of Matlab. The *bwlabel* and *stats* functions were used to define and record the properties of objects in successive cross-sectional images. The area for each object was obtained in each binary image slice, and objects less than fifty percent of the area of the largest object were discarded since distributions of WSS in the external iliac arteries were the focus of the current investigation. The iliac artery bifurcation was defined as the location where the number of objects increased from 1 to 2. The location of the centroids of each object were then calculated and used to delineate between objects in each main iliac arterial branch. Objects in successive cross-sectional slices were assigned to branches based on the minimum distance of the centroids corresponding to objects in the current slice with respect to those in the previous slice. The Sobel method of edge detection was then applied in Matlab to create arrays corresponding to points along the edge of each artery. This process of branch determination, location and edge definition was robust for reconstructed volumes and did not fail during processing of any volumes in the current report.

The coordinates corresponding to each slice of the iliac arteries were spatially aligned for use with automated smoothing and CFD

Computer Methods and Programs in Biomedicine, Vol. 79, No. 2 (August 2005): pg. 121-134. DOI.

mesh generation programs. Coordinates representing the slices that comprised each vessel were centered about the origin and divided into quadrants. The coordinates in each quadrant were sorted in the *y* followed by the *x* axis to proceed clockwise. The points in each quadrant were then combined into a common matrix and once again centered about the midline of each iliac artery.

Circumferential and axial smoothing were performed according to previously described methods[15]. Briefly, radius arrays were created for each iliac artery slice and smoothed using a mean filter in Matlab. The radius values were then interpolated to reflect the desired number of circumferential points that comprise the computational vessel. Modification of the axial resolution was also integrated into this portion of the vascular geometry extraction process for use in the investigation of mesh independence during CFD modeling. An axial resolution of 1 indicated that each slice of the reconstructed volume was used during CFD mesh generation. Similarly, an axial resolution of 2 indicated that every other slice was used. The angular increment between circumferential points was uniform as a result of the sorting algorithm discussed above. This allowed for axial arrays corresponding to each circumferential point to be easily created and smoothed. Smoothing was performed by converting from Cartesian to polar coordinates and using the smoothing function in Matlab[15]. After conversion back into Cartesian coordinates, this method was found to eliminate errors introduced along the length of a vessel during reconstruction while conserving the geometric properties of the artery.

2.5. CFD mesh generation of reconstructed iliac arteries

Radius values from reconstructed iliac arteries were imported into a custom designed automated mesh generation program in Matlab after surface smoothing. Additional length (AL) was added to each artery to allow for fully developed flow using the equation: $AL = 0.06 \cdot Re \cdot d$, where *Re* is the Reynolds number and *d* is the vessel inlet diameter[16]. The radius values for the added inlet length were constant and equal to the average radius of the first slice of each iliac artery. A 50:50 flow split was assumed for all computational arteries[17] and was confirmed from in vivo blood flow velocity measurements obtained using precalibrated ultrasonic flow probes placed around the

proximal iliac arteries (data not shown). Thus, inlet length was added purely in the *z*-direction to mimic the shape of the velocity profile at the inlet of the iliac arteries, without modeling the proximal descending aorta. This assumption provided the advantage of having more computational nodes and improved spatial resolution within the distal stented region of the artery. The radius values for the additional length at the outlet were equal to those of the last arterial slice.

Computational meshes for stented iliac arteries were generated by combining the low and high magnification reconstructions. Spatially equivalent regions several millimeters proximal and distal to the stented region were identified within the low and high magnification projection images. Radius values bounded by this identifying region within the smoothed and processed low magnification reconstruction volumes were then digitally replaced by those of the equivalent region obtained after processing of the high magnification reconstruction volumes. This process facilitated the creation of very fine computational meshes that were required to capture subtle variations on the surface of the vascular casts. Thus, the resolution proximal and distal to the stented region was moderately reduced and arbitrary interface boundary conditions were implemented using the commercially available software package CFD-ACE (CFDRC; Huntsville, AL) to increase the circumferential and axial resolution within the stented region to approximately 32 and 50 microns, respectively. Establishing arbitrary interfaces facilitated the computational extrusion of the vessel distal and proximal to the stent and allowed for the use of different circumferential resolutions within a structured mesh environment. Arbitrary interfaces generated within the CFD environment conformed to suggestions outlined in the user manual of CFD-ACE. This software uses a finite volume approach to solve the Navier-Stokes, continuity and conservation of energy equations at the center of each hexahedral control volume.

2.6. Validation of post-processing operations

The potential error in distributions of WSS introduced by surface smoothing was investigated using a theoretical artery in which the vessel radius was varied in a sinusoidal pattern along the length of the vessel. A high frequency component was also superimposed on the

Computer Methods and Programs in Biomedicine, Vol. 79, No. 2 (August 2005): pg. 121-134. DOI.

axially varying radius to produce a computational vessel containing spatial error equivalent to that obtained after high magnification reconstruction of the polyethylene tube phantom (Fig. 4). Distributions of WSS in the theoretical and high frequency spatial error arteries were determined after imposing a steady-state inlet velocity of 24 mm/s (*Re* = 17) similar to that used at the inlet of the reconstructed iliac arteries. Theoretical arteries in the absence and presence of high frequency spatial error were then subjected to the surface smoothing techniques described above and distributions of WSS were obtained as previously described[3,4].

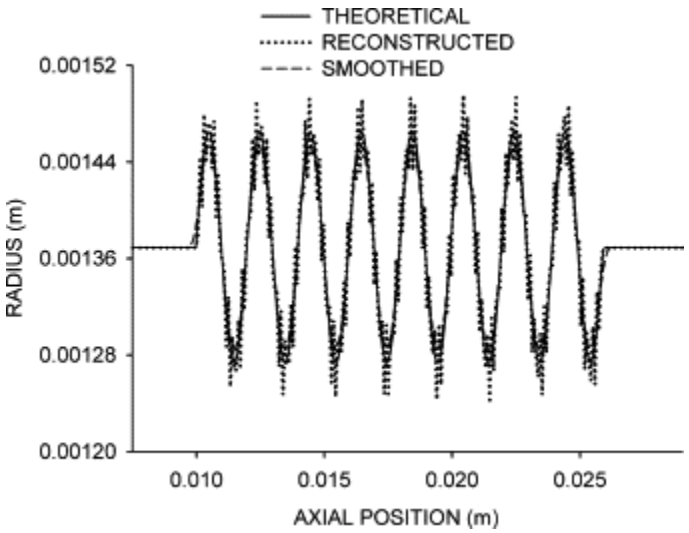

Fig. 4. Axial radii from a theoretical artery (solid line) and an artery with spatial error equivalent to that resulting from high magnification image reconstruction before (dotted line) and after (dashed line) implementation of the surface smoothing techniques discussed in the text.

Development of regional neointimal hyperplasia within the stented portion of an artery may introduce localized geometric asymmetry. As a result, we also determined the frequency of surface perturbations that could be resolved after application of the surface smoothing techniques presented above. To address this question, four theoretical arteries were created with various sinusoidal surface perturbation frequencies (4, 8, 12 and 16) having a magnitude equal to a single stent strut (96 microns). Each idealized computational vessel contained a 16 mm perturbation region and was subjected to an inlet velocity boundary condition of 24 mm/s. Distributions of WSS were determined for each artery before and after surface smoothing, and the resulting disparity was calculated by dividing distributions of

Computer Methods and Programs in Biomedicine, Vol. 79, No. 2 (August 2005): pg. 121-134. DOI.

WSS obtained in the smoothed artery by those in the theoretical artery.

3. Results

3.1. Microfocal X-ray computed tomography and vascular reconstruction

An averaged projection image obtained from one of 360 imaging planes is illustrated in Fig. 3. Low and high magnification reconstruction volumes obtained from stented and normal iliac arteries are depicted after rendering in Fig. 5. The image acquisition duration for each reconstruction volume was approximately 6 min and reconstruction of the 360 2D images took approximately 6 h on a 1.8 MHz Compaq Presario 920US laptop computer with 1 Gbyte of RAM.

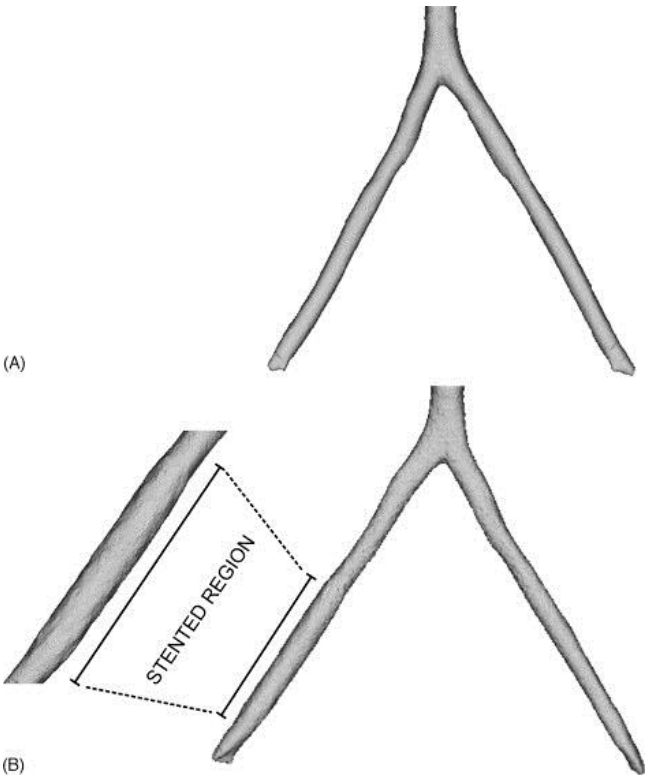

Fig. 5. Representative normal (A) and stented iliac arteries (B) reconstructed using the Feldcamp cone-beam algorithm. Rendering of a high magnification reconstruction obtained within the stented region is also illustrated in the insert of B.

Computer Methods and Programs in Biomedicine, Vol. 79, No. 2 (August 2005): pg. 121-134. DOI.

3.2. Reconstructed vascular geometry extraction

Unprocessed cross-sectional slices from the reconstruction volume of an iliac artery cast contained a modest amount of circular streaking due to detector pixels with non-linear gain or non-zero offset characteristics (Fig. 6A). The RAR algorithm substantially attenuated these circular artifacts but also preserved the integrity of the data within the reconstruction volume (Fig. 6B). The processes of automated thresholding for identification of the arterial wall, spatial sorting of points along the luminal surface, and circumferential and axial surface smoothing are illustrated in Fig. 7. These post-processing operations were completed after approximately 15 min for each reconstruction volume. The guidelines outlined in the Section 2 were used in conjunction with the techniques discussed in Section 2.4 to smooth a polyethylene 240 tube phantom as illustrated in Fig. 8. The surface smoothing procedure was considered acceptable when imposing a steady-state velocity value resulted in relatively small deviations in axial and circumferential normalized WSS (1.001 ± 0.050). These deviations were similar to those previously described (1.099 ± 0.043)[10].

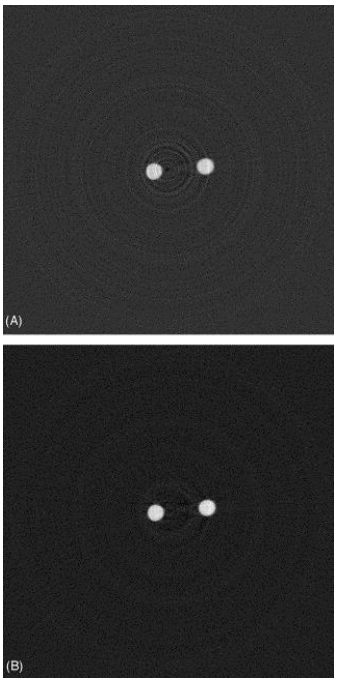

Fig. 6. Panels illustrating a cross-sectional slice from the reconstruction volume of an iliac artery cast before (A) and after (B) implementation of a ring artifact reduction algorithm.

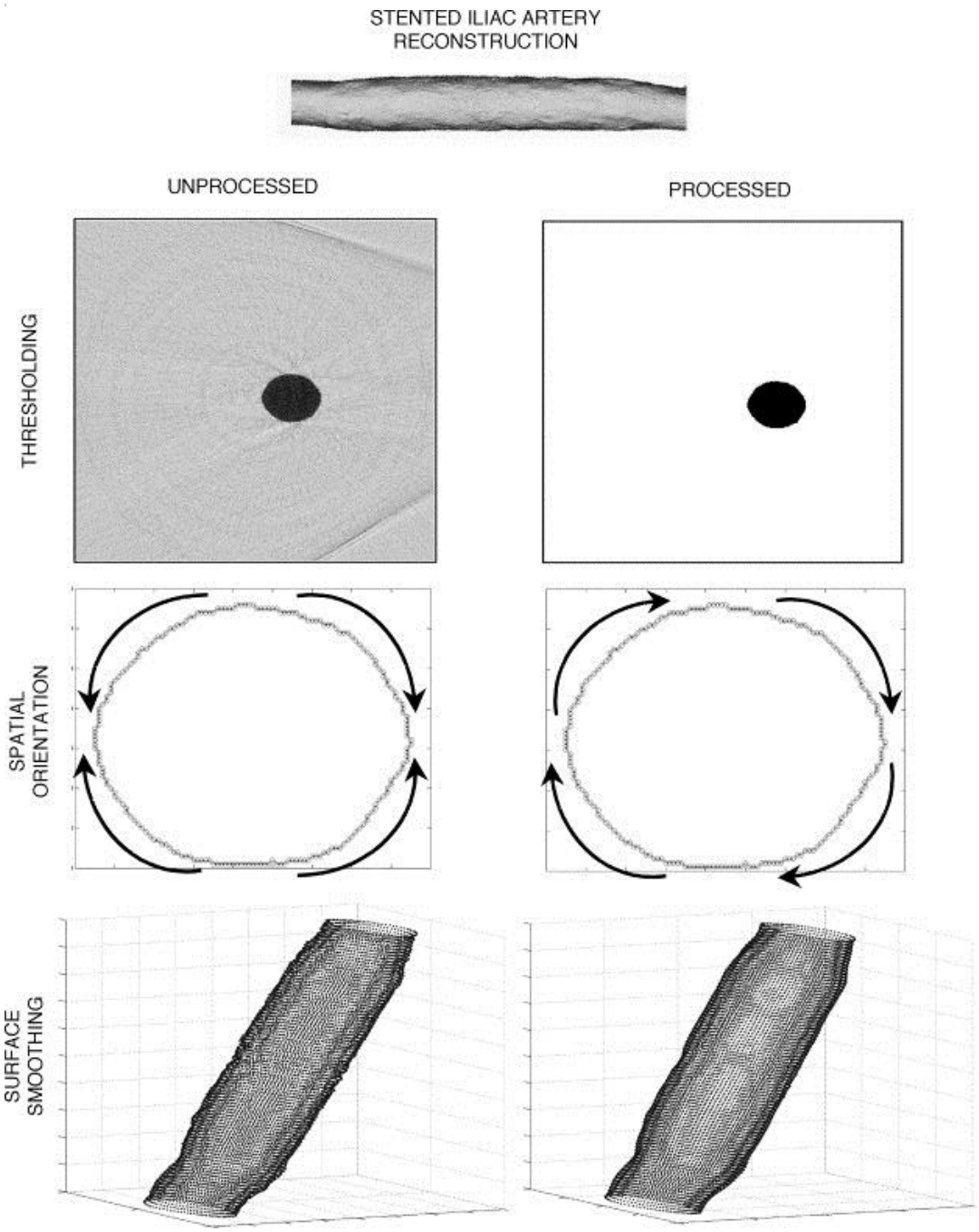

Fig. 7. Panels illustrating the automated processing of normal and stented iliac artery reconstructions performed in MATLAB. Reconstructed iliac arteries were subjected to thresholding for identification of the arterial wall, spatial sorting of points along the luminal surface and circumferential and axial surface smoothing.

Computer Methods and Programs in Biomedicine, Vol. 79, No. 2 (August 2005): pg. 121-134. DOI.

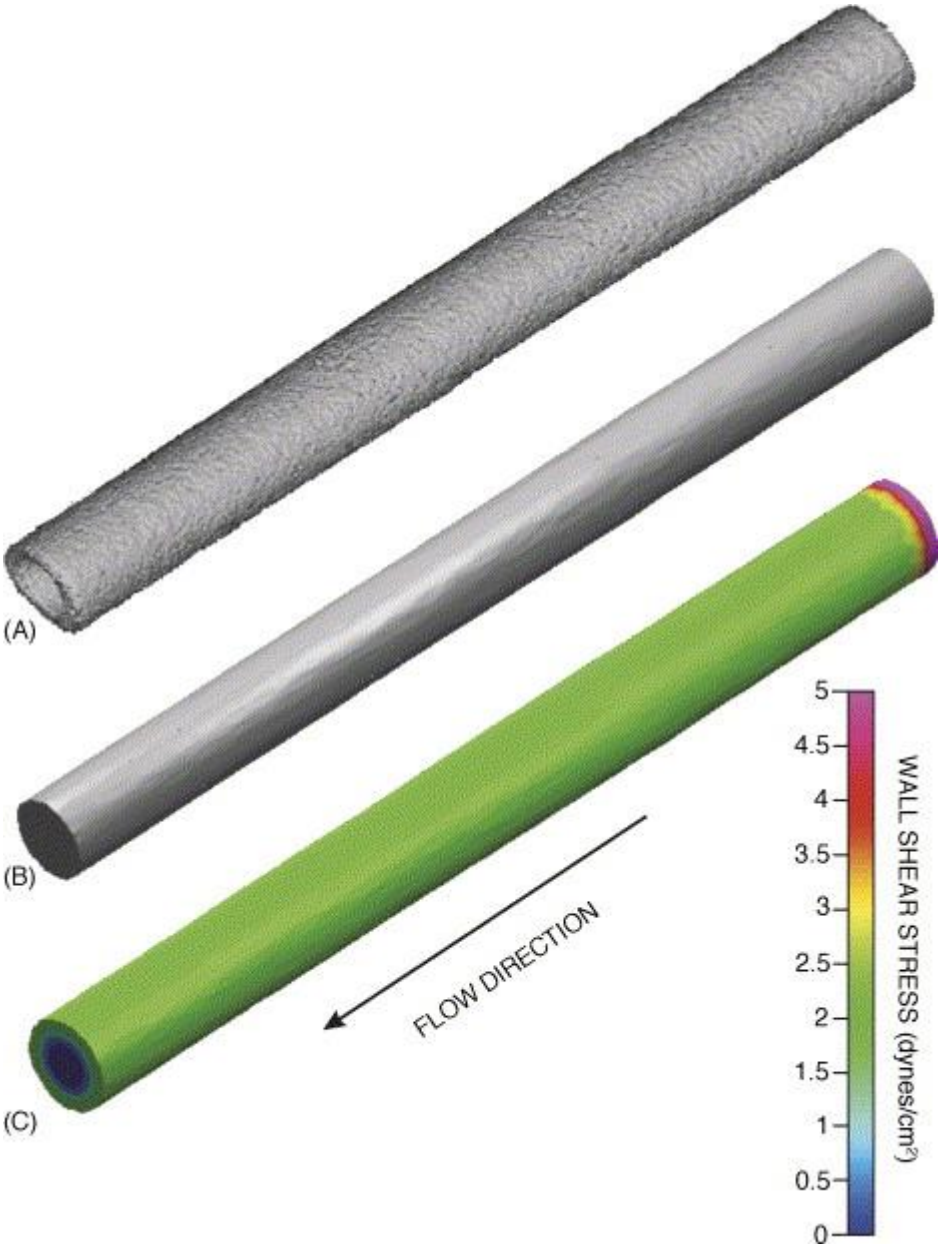

Fig. 8. Surface smoothing of a reconstructed polyethylene tube. Illustrations of a rendered polyethylene tube obtained before (A) and after (B) implementation of the surface smoothing operations discussed in the text. The uniformity of WSS distributions along the wall of the reconstructed and smoothed polyethylene tube is depicted in (C).

3.3. CFD mesh generation of reconstructed iliac arteries

The flow domains of unstented and stented iliac arteries obtained from microfocal X-ray CT imaging, reconstruction, and post-

processing are depicted in Fig. 9. The number of nodes dedicated to CFD mesh generation of stented iliac arteries was 588,214 ± 71,603 (mean ± S.D.) and varied according to the size of the casted iliac artery. Computational vessels were created in approximately 1 h using the automated mesh generation program developed in Matlab. Distributions of WSS are presented in Fig. 10. Reductions in normalized WSS within the stented region were produced concomitant with the increased luminal diameter of the stent. Increases in the spatial disparity of WSS due to the intricacies of the stent were temporally alleviated after 21 days after implantation.

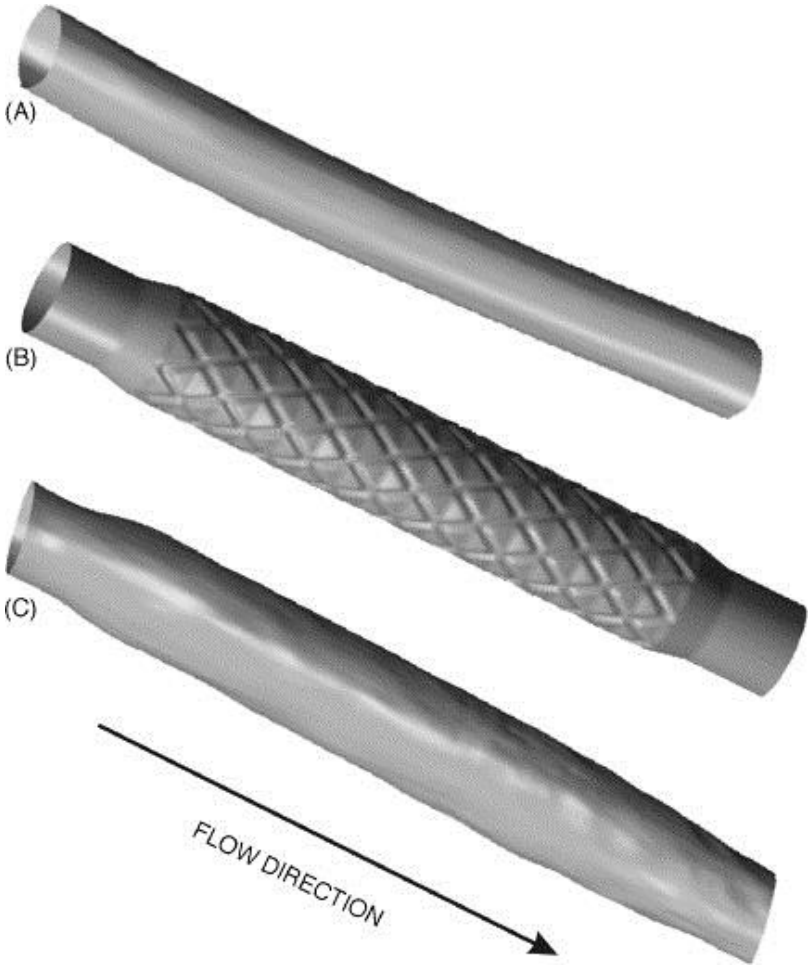

Fig. 9. Representative computational geometries of the reconstructed iliac artery flow domain. The in vivo flow domain in a normal artery (A), an acutely stented theoretical vessel (B), and a stented artery 21 days after implantation (C).

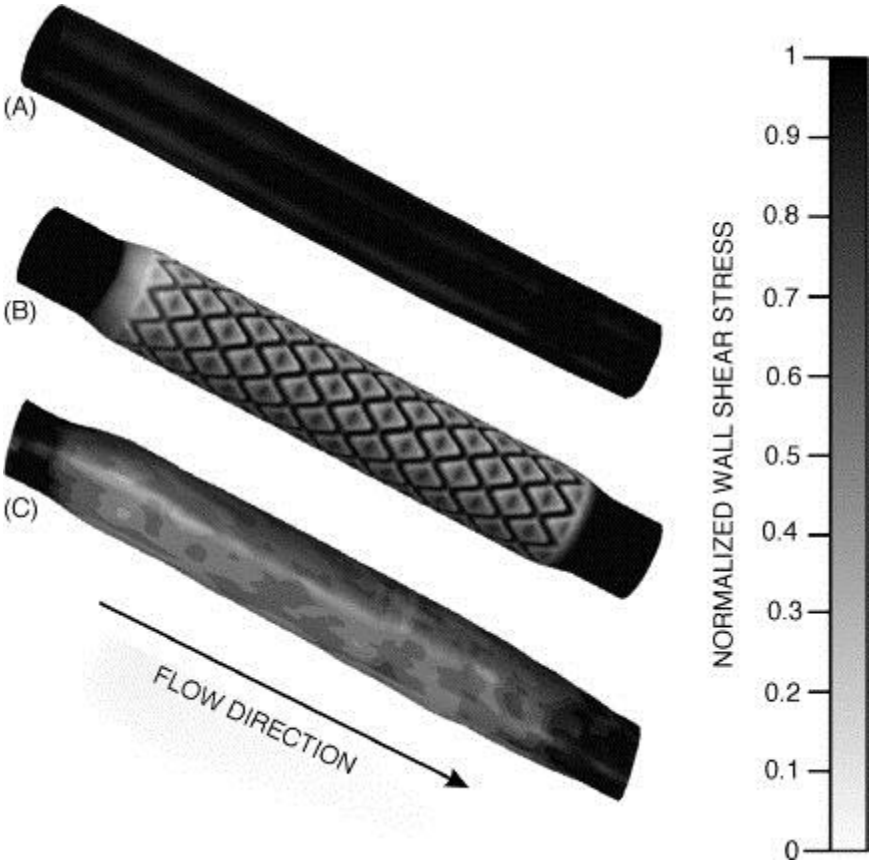

Fig. 10. Representative distributions of normalized WSS in normal and stented iliac arteries. The in vivo distributions of WSS in a normal artery (A), an acutely stented theoretical vessel (B) and a stented artery 21 days after implantation (C).

3.4. Validation of post-processing operations

Distributions of WSS obtained from theoretical arteries in the absence and presence of high frequency spatial error subjected to the surface smoothing techniques are illustrated in Fig. 11. Surface smoothing of the artery with high frequency spatial error causes a modest amount of WSS attenuation as compared to the theoretical artery. The coefficient of variation defined as the standard deviation of the squared error divided by the mean theoretical distribution of WSS was 0.52%.

Computer Methods and Programs in Biomedicine, Vol. 79, No. 2 (August 2005): pg. 121-134. DOI.

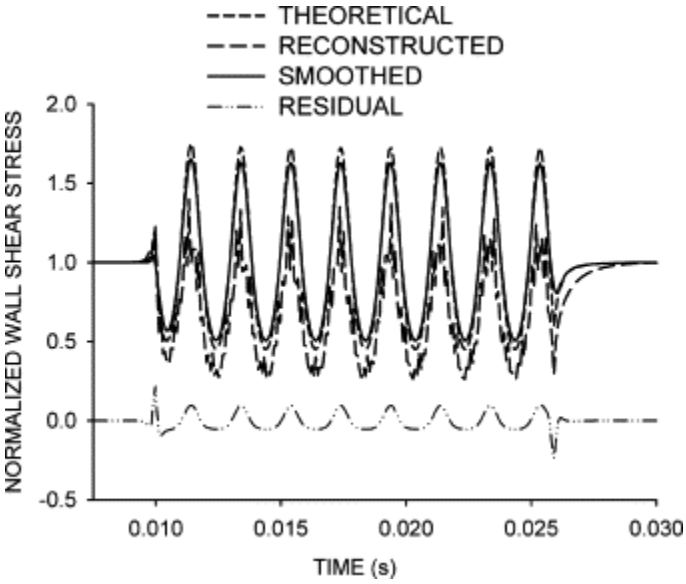

Fig. 11. Normalized distributions of WSS in a theoretical artery and those obtained before and after surface smoothing of an artery with spatial error equivalent to that resulting from high magnification image reconstruction. The residual calculated as the difference between distributions of WSS in theoretical and smoothed arteries is also presented.

The disparity between distributions of WSS obtained from theoretical vessels containing 4, 8, 12 or 16 surface perturbations before and after smoothing was expressed as a function of the perturbation number and represents the transfer function of the series of post-processing operations outlined above (Fig. 12). The transfer function for the current system containing reconstructed 16 mm stents implanted into rabbit iliac arteries for up to 21 days and resolved at circumferential and axial resolutions of 32 and 50 microns, respectively, indicated a modest decline in WSS accuracy at increasing frequencies. A representative axial distribution of normalized WSS with approximately 8 transients along the vessel lumen (Fig. 13) demonstrated that distributions of WSS were resolved with 96% accuracy by the transfer function of the surface smoothing operations implemented in the current investigation (e.g. 8 transients for a 16 mm stent length corresponds to a frequency of 0.5 and the transfer function at this frequency is 0.96).

Computer Methods and Programs in Biomedicine, Vol. 79, No. 2 (August 2005): pg. 121-134. DOI.

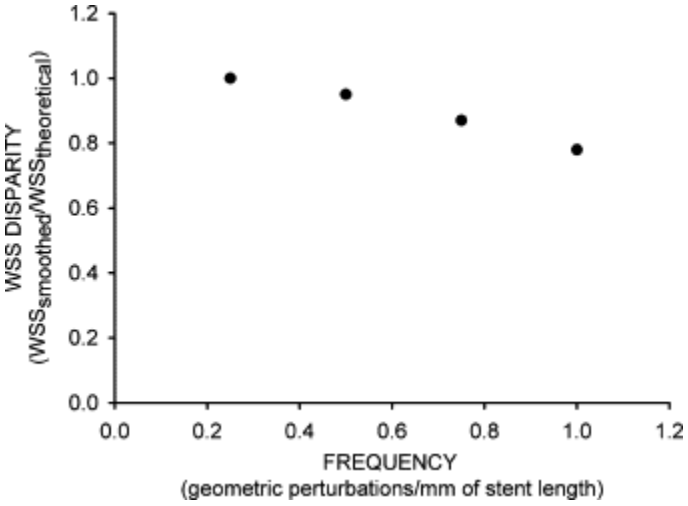

Fig. 12. Transfer function describing the relationship between wall shear stress accuracy and surface perturbation frequency in reconstructed iliac arteries up to 21 days after stent implantation. Distributions of WSS were determined for arteries containing 4, 8, 12 and 16 perturbations over a 16 mm region before and after smoothing according to the techniques presented in the text. WSS disparity was calculated by dividing distributions of WSS obtained in the smoothed artery by those in the theoretical artery.

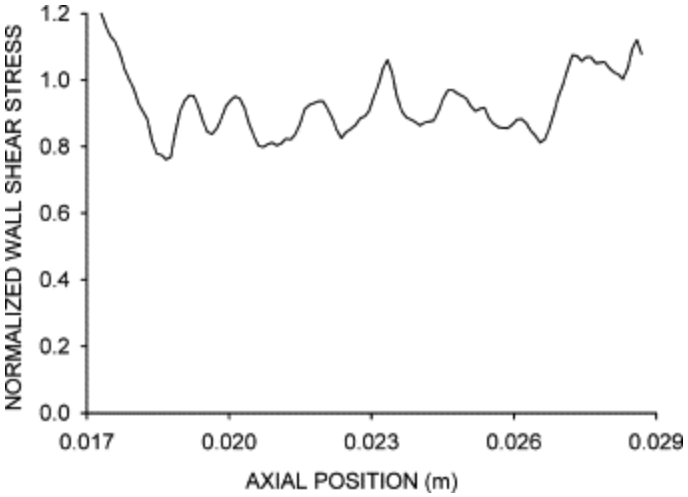

Fig. 13. Representative axial distributions of normalized wall shear stress in the stented portion of an iliac artery demonstrating the ability of the post-processing operations to successfully resolve perturbations within the stented region of the vessel.

4. Discussion

Vascular geometry influences the local distribution of WSS. Branching and curvature alter the ideal blood flow environment and correlate with sites of neointimal hyperplasia[2,18,19]. Rates of restenosis

after stent implantation vary with stent design, and stent geometry has been identified as an important clinical predictor of neointimal hyperplasia[1,20]. We have recently reported that the stent-to-artery deployment ratio and the diameter and width of the stent linkages differentially affect the area of the vessel subjected low WSS and elevated spatial WSS gradients using a 3D CFD model of a coronary artery[3]. These data suggest that modest geometric disparity between the region of the implanted stent and the native vessel influence distributions of WSS and may be associated with the development of neointimal hyperplasia after implantation. However, the spatial and temporal impact of the local stent geometry on indices of WSS remains to be evaluated in vivo and may account for the disparity in restenosis rates among differing stent designs. In vivo studies conducted in this area cannot yield meaningful data unless accurate computational representations of the arterial environment into which a stent is implanted are established. In the current report, we presented the details and limitations of a series of post-processing operations that can be used in conjunction with microfocal X-ray CT imaging and reconstruction to generate accurate flow domains within the localized region of a stent several weeks after implantation. Studies conducted in our laboratory using these techniques have indicated that temporal alterations in distributions of WSS after stent implantation in vivo may spatially correlate with the development of neointimal hyperplasia within the interventional region.

The transfer function obtained from the series of post-processing operations performed after microfocal X-ray CT imaging (Fig. 12) in the current report is dependent on the spatial mesh density within the stented region, and also provided important information about the confidence of WSS patterns generated for reconstructed arteries. The current transfer function containing reconstructed 16 mm stents implanted into rabbit iliac arteries for up to 21 days after implantation and resolved at circumferential and axial resolutions of 32 and 50 microns, respectively, indicated that the present post-processing techniques are sufficient to resolve distributions of WSS with at least 80% accuracy in stented vascular segments containing 16 surface perturbations over a 16 mm axial region. Distributions of WSS were resolved with 96% accuracy in a model of chronic antegrade iliac artery stent implantation developed in

Computer Methods and Programs in Biomedicine, Vol. 79, No. 2 (August 2005): pg. 121-134. DOI.

our laboratory and used in the current investigation as the slotted-tube stents implanted contain eight repeating strut units.

The current method for replicating distributions of WSS in vivo used the desirable spatial accuracy of microfocal X-ray CT imaging and reconstruction with relatively simple, unbiased and precise post-processing algorithms that accurately produced flow domains corresponding to in vivo distributions of WSS with errors on the order of those previously reported[10]. Our data using these post-processing operations demonstrate that reductions in normalized WSS and the increased spatial disparity of distributions of WSS immediately after stent implantation are temporally alleviated due to the development of neointimal hyperplasia within this region. These results concur with our histological findings within the stented region that have been shown to correlate closely with temporal alterations in spatial distributions of WSS and elevated spatial wall shear stress gradients[7].

The present methods contain several potential limitations that require further consideration. Ideally, the bifurcation of the distal aorta into the proximal iliac arteries should be computationally represented to replicate the developing flow profiles in the proximal region of the iliac arteries. However, this bifurcation was not modeled using the current methodology. Instead, we performed independent modeling of contralateral stented and unstented iliac arteries equipped with additional length at the inlet and outlet of each vessel to approximate the flow profiles in these regions, and allow for increased spatial resolution within the stented region. Wall shear stress values in the distal region of the iliac artery where stent implantation occurred are well removed from the inlet of the vessel. Thus, modest deviations from the actual inlet velocity profile caused by this assumption probably have little impact on distributions of WSS in the stented portion of the artery.

The transfer function presented here describes the limitations of applying the current post-processing methods to the microfocal X-ray CT imaging reconstruction data sets of iliac arteries implanted with 16 mm stents designed with eight repeating strut units. Thus, the transfer function may not be applicable for stents of differing lengths or designs applied in similar or geometrically different arterial segments. Nevertheless, analyses similar to those presented in this

Computer Methods and Programs in Biomedicine, Vol. 79, No. 2 (August 2005): pg. 121-134. DOI.

report may also be conducted with longer or shorter stents of various designs using the techniques presented here.

5. Conclusion

In summary, we report the details of a series of post-processing operations designed to optimize microfocal X-ray computed tomography-derived reconstruction volumes. This technique allows investigation of the influence of stent-induced alterations in indices of WSS on neointimal hyperplasia in vivo. This report documents methods to identify alterations in WSS obtained from the flow domain within stented vessels in vivo at a resolution sufficient to detect subtle alterations in vascular geometry. The results demonstrate that the current techniques are suitable for classifying alterations in indices of WSS after stent implantation in vivo. These techniques will be used in subsequent studies in our laboratory to test the hypothesis that spatial alterations in distributions of WSS after stent implantation in vivo may spatially correlate with the temporal development of neointimal hyperplasia within the stented region.

Acknowledgements

This work was supported in part by National Institutes of Health grants HL-03690 (to Dr. Kersten), HL-63705 (to Dr. Kersten), HL-54820 (to Dr. Warltier), and GM-08377 (to Dr. Warltier) from the United States Public Health Service, Bethesda, Maryland.

References

[1] A. Kastrati, J. Mehilli, J. Dirschinger, J. Pache, K. Ulm, H. Schuhlen, M. Seyfarth, C. Schmitt, R. Blasini, F.J. Neumann, A. Schomig. Restenosis after coronary placement of various stent types. *Am. J. Cardiol*., 87 (1) (2001), pp. 34–39

[2] D.N. Ku, D.P. Giddens, C.K. Zarins, S. Glagov. Pulsatile flow and atherosclerosis in the human carotid bifurcation. Positive correlation between plaque location and low oscillating shear stress. *Arteriosclerosis*, 5 (3) (1985), pp. 293–302

[3] J.F. LaDisa, L.E. Olson, I. Guler, D.A. Hettrick, S.H. Audi, J.R. Kersten, D.C. Warltier, P.S. Pagel. Stent design properties and deployment ratio influence indexes of wall shear stress: a three-dimensional computational fluid dynamics investigation within a normal artery. *J. Appl. Physiol*., 97 (2004), pp. 424–430

[4] J.F. LaDisa Jr., I. Guler, L.E. Olson, D.A. Hettrick, J.R. Kersten, D.C. Warltier, P.S. Pagel. Three-dimensional computational fluid dynamics modeling of alterations in coronary wall shear stress produced by stent implantation. *Ann. Biomed. Eng*., 31 (8) (2003), pp. 972–980

[5] F.J. Gijsen, R.M. Oortman, J.J. Wentzel, J.C. Schuurbiers, K. Tanabe, M. Degertekin, J.M. Ligthart, A. Thury, P.J. de Feyter, P.W. Serruys, C.J. Slager. Usefulness of shear stress pattern in predicting neointima distribution in sirolimus-eluting stents in coronary arteries. *Am. J. Cardiol*., 92 (11) (2003), pp. 1325–1328

[6] J.J. Wentzel, D.M. Whelan, W.J. van der Giessen, H.M. van Beusekom, I. Andhyiswara, P.W. Serruys, C.J. Slager, R. Krams. Coronary stent implantation changes 3D vessel geometry and 3D shear stress distribution. *J. Biomech*., 33 (10) (2000), pp. 1287–1295

[7] J.F. LaDisa Jr., L.E. Olson, R.C. Molthen, D.A. Hettrick, M.D. Hardel, P.F. Pratt, J.R. Kersten, D.C. Warltier, P.S. Pagel. Alterations in wall shear stress predict sites of neointimal hyperplasia after stent implantation in rabbit iliac arteries. *Am. J. Physiol. Heart Circ. Physiol*., 288 (2005), pp. 2465–2475

[8] K.L. Karau, R.H. Johnson, R.C. Molthen, A.H. Dhyani, S. Haworth, C. Hanger, D. Roerig, C.A. Dawson. Microfocal X-ray CT imaging and pulmonary arterial distensibility in excised rat lungs. *Am. J. Physiol. Heart Circ. Physiol*., 281 (2001), pp. H1447–H1457

[9] K.L. Karau, R.C. Molthen, A. Dhyani, S.T. Haworth, C.C. Hanger, D.L. Roerig, R.H. Johnson, C.A. Dawson. Pulmonary arterial morphometry from microfocal X-ray computed tomography. *Am. J. Physiol. Heart Circ. Physiol*., 281 (6) (2001), pp. H2747–H2756

[10] J.A. Moore, D.A. Steinman, C.R. Ethier. Computational blood flow modelling: errors associated with reconstructing finite element models from magnetic resonance images. *J. Biomech*., 31 (1998), pp. 179–184

[11] J.F. LaDisa Jr., H.T. Meier, L.E. Olson, J.R. Kersten, D.C. Warltier, P.S. Pagel. Antegrade iliac artery stent implantation for the temporal and spatial examination of stent-induced neointimal hyperplasia and alterations in regional fluid dynamics. *J. Pharmacol. Toxicol. Meth*., 51 (2005), pp. 115–121

[12] J.G. Myers, J.A. Moore, M. Ojha, K.W. Johnston, C.R. Ethier. Factors influencing blood flow patterns in the human right coronary artery. *Ann. Biomed. Eng*., 29 (2001), pp. 109–120

[13] L.A. Feldkamp, L.C. Davis, J.W. Kress. Practical cone-beam algorithm. *J. Opt. Soc. Am*., 1 (6) (1984), pp. 612–619

[14] M.L. Rivers, S. Sutton, P. Eng. Geoscience applications of X-ray computed microtomography. *Proceedings of SPIE, Developments in X-ray Tomography II*, vol. 3772 (1999), pp. 78–86

[15] Q. Long, X.Y. Xu, M.W. Collins, M. Bourne, T.M. Griffith. Magnetic resonance image processing and structured grid generation of a human abdominal bifurcation. *Comp. Meth. Prog. Biomed*., 56 (1998), pp. 249–259

[16] R.W. Fox, A.T. McDonald. *Introduction to Fluid Mechanics*. (4th ed.) John Wiley & Sons Inc., New York (1992)

[17] J.A. Moore, B.K. Rutt, S.J. Karlik, K. Yin, C.R. Ethier. Computational blood flow modeling based on in vivo measurements. *Ann. Biomed. Eng*., 27 (1999), pp. 627–640

[18] A.M. Malek, S.L. Alper, S. Izumo. Hemodynamic shear stress and its role in atherosclerosis. *JAMA: J. Am. Med. Assoc*., 282 (21) (1999), pp. 2035–2042

[19] J.E. Moore Jr., C. Xu, S. Glagov, C.K. Zarins, D.N. Ku. Fluid wall shear stress measurements in a model of the human abdominal aorta: oscillatory behavior and relationship to atherosclerosis. *Atherosclerosis*, 110 (2) (1994), pp. 225–240

[20] Y. Yoshitomi, S. Kojima, M. Yano, T. Sugi, Y. Matsumoto, M. Saotome, K. Tanaka, M. Endo, M. Kuramochi. Does stent design affect probability of restenosis? A randomized trial comparing multilink stents with GFX stents. *Am. Heart J.,* 142 (3) (2001), pp. 445–451

*Corresponding author at: Medical College of Wisconsin, MEB-M4280, 8701 Watertown Plank Road, Milwaukee, WI 53226, USA. Tel.: +1 414 456 5733; fax: +1 414 456 6507.